https://doi.org/10.15407/ujpe70.5.287

O.S. POTIIENKO,[1] D.V. ZHURAVEL,[2] N.O. CHUDAK,[1] D.M. RIABOV[3]

[1] Odesa Polytechnic National University
*(1, Shevchenko Ave., Odesa 65044, Ukraine; e-mail: frumle@ukr.net)*
[2] Bogolyubov Institute for Theoretical Physics, Nat. Acad. of Sci. of Ukraine
*(14b, Metrolohichna Str., Kyiv 03143, Ukraine)*
[3] State University of Intelligent Technologies and Telecommunications
*(1, Kuznechna Str., Odesa 65023, Ukraine)*

# SIMULATION OF SINGLE DIFFRACTION DISSOCIATION IN RESONANCE REGION AT LHC ENERGIES

*The single diffraction dissociation duality-based model is studied at low missing masses in the light of new experimental data. The distinguishing feature of the model is the nonlinear Regge proton trajectory used to account for the resonances contributions to the cross-sections. It helps to classify and understand the spectrum of excited states of a proton and their decays, providing insights into the internal structure and dynamics of particles. The behavior of the differential cross-section in the resonance region at small missing masses $M_x$ is investigated. All other resonances that are not taken into account are modeled using the constant background contribution. The possibility and correctness of such a choice is discussed. The model parameters are refined in the light of new experimental data.*

*K e y w o r d s*: single diffraction dissociation, structure function of a proton, resonance region, low missing masses, cross-section, event generation.

## 1. Introduction

As is known from many experimental results [1], in the processes of hadron scattering at high energies, the majority of events are concentrated in the region of small momentum transfers. The combination of high energies and small momentum transfers creates conditions for the realization of diffraction processes [2, 3]. Diffraction in particle physics draws an analogy from classical wave diffraction, where waves encounter an obstacle and spread out. Similarly, in diffractive dissociation, a hadron such as a proton encounters another particle or nucleus, leading to its partial or complete dissociation. The process is characterized by a small momentum transfer between the incident particle and the target, resulting in a "rapidity gap" – a region in the detector with very few or no particles. One of the significant findings from diffractive dissociation studies is the confirmation of the pomeron exchange model, which has been supported by experimental data showing characteristic rapidity gaps in diffractive events. The detailed measurements of diffractive cross-sections and the kinematic distributions of final-state particles have provided insights into the non-perturbative aspects of QCD.

The main types of diffractive processes are the single dissociation (SD), double dissociation (DD), and

C i t a t i o n: Potiienko O.S., Zhuravel D.V., Chudak N.O., Riabov D.M. Simulation of single diffraction dissociation in resonance region at LHC energies. *Ukr. J. Phys.* **70**, No. 5, 287 (2025). https://doi.org/10.15407/ujpe70.5.287.

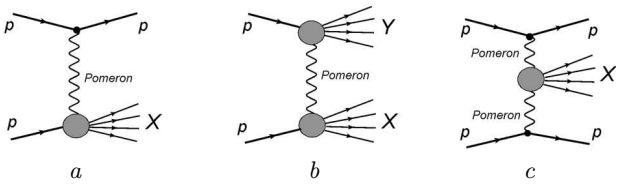


***Fig. 1.*** The main types of diffractive processes: single dissociation (SD) ($a$), double dissociation (DD) ($b$), and central diffraction (CD)($c$), where $p$ – is the proton, $X(Y)$ – is a system of secondary hadrons

central diffraction (CD) (Fig. 1). Diffraction dissociation has been studied in various high-energy physics experiments, such as TOTEM [4], CMS [5], CERN [6–8], ALICE [9] and ATLAS [10]. In this work, we will consider the low-mass single diffraction dissociation of protons. The small missing masses $M_X$ show a multitude of peaks or features corresponding to different nucleon resonances [11]. Nucleon resonances are essential for understanding the strong force interactions described by QCD.

The experimentally observed characteristics of the diffraction dissociation largely depend on the properties of the hadron-region vertex. We will consider this vertex as the amplitude of a real process. Using the unitarity condition [12], duality [13], this amplitude can be calculated as the sum of the resonance contributions known from experiments [14]. In this work, we examined the exchange of a single pomeron. This pomeron is typically considered to be a simple pole of the partial scattering amplitude. However, there are other dynamic models, such as the model with exchange of a pomeron-like analog, but with an odd signature [15, 16], and the dipole pomeron model, which is the foundation, further enhanced by incorporating a dip-bump mechanism [17]. Therefore, it is of interest to explore the combination of different models of the hadron-reggeon vertex and collision dynamics to describe experimental data. In this work, we present the results of fits with the exchange of a single pomeron pole.

Our goal is to calculate the differential cross-section $d\sigma/dt$ of single diffraction dissociation within the resonance region at small missing masses $M_X$ and the total single diffraction dissociation cross section.

The structure of the article is presented as follows. In Section 2, we will find the structure function of a proton $W_2\left(M_X^2, t\right)$, which is related to the imaginary part of the dual-Regge transition amplitude $A\left(M_X^2, t\right)$. In Section 3, we will show that the behavior of the cross-section is influenced by baryon resonances. In Section 4, we calculate total and differential cross-sections and fit them to the experimental data. In Section 5, we compare the considered model with the MBR methods in the resonance region at low missing masses.

## 2. From Elastic Scattering to Single Diffractive Dissociation

Let us consider the diffractive dissociation $p + p \to \to p + X$, where $p$ is a proton, $X$ is a system of secondary hadrons. This process is represented as a similar elastic process, where $X$ is considered as a single particle with a squared mass $M_X^2$, which equals the scalar square of the sum of the four-momenta of $X$. Then, instead of the elastic scattering amplitude, we obtain the amplitude of diffractive dissociation with the vertices of the reggeon-hadron interaction. Such modification [11] leads to the expression (1) for the differential cross-section of single diffraction dissociation at large $s$ (the square of the center-of-mass energy of the collision)

$$\frac{d\sigma_{\mathrm{SD}}}{dtdM_x^2} \approx \frac{9\beta^4}{4\pi}\left[F^p\left(t\right)\right]^2\left(\frac{s}{M_x^2}\right)^{2\alpha_p(t)-2}\frac{W_2\left(t, M_x^2\right)}{2m}, \quad (1)$$

where $t$ is the momentum transfer between colliding particles, $\beta$ is the quark-Pomeron coupling, $m$ is the proton mass, $\alpha_P\left(t\right)$ is a vacuum Regge trajectory, $F^p\left(t\right)$ is the elastic form factor of the proton, $W_2\left(t, M_x\right)$ is the structure function of a proton, which describes the Pomeron-proton vertex. According to [11, 18], we take the Pomeron trajectory $\alpha_P\left(t\right) = = 1.08 + 0.25t$. The expression for the proton elastic form factor is given by $F^p\left(t\right) = \left(1.0 - t/0.71\right)^{-2}$.

The most challenging building block of the expression (1) is the structure function $W_2\left(t, M_x^2\right)$.

Following [11], this structure function can be constructed from the similarity between the Pomeron-proton diffractive proccess $\mathbb{P}p \to X$ (Pomeron denoted by $\mathbb{P}$) and deep inelastic scattering process $\gamma^* p \to X$ (Fig. 2). Let us briefly highlight the major steps on the way to $W_2\left(M_X^2, t\right)$:

### 2.1. Step 1: Similarity with $\gamma^* p \to X$

We utilize the similarity between the inelastic vertices $\mathbb{P}p \to X$ and $\gamma^* p \to X$ and the corresponding structure functions. The structure functions $F_2\left(x, Q^2\right)$ for

$\gamma^* p$ processes have been studied in [19] and are connected [20] with $W_2$ through the following relation:

$$\nu W_2\left(M_X^2, t\right) = F_2\left(x, t\right), \tag{2}$$

where $\nu = \left(M_X^2 - m^2 - t\right)/2m$ is another kinematic variable. Thus, establishing an analogy between the virtual photon $\gamma^*$ and the Pomeron ($\mathbb{P}$) and setting $Q^2 = -t$, yields

$$\nu W_2\left(M_X^2, t\right) = F_2\left(x, t\right) = \\ = \frac{-4t(1-x)^2}{\alpha_{fs}\left(M_X^2 - m^2\right)\left(1 - 4m^2x^2/t\right)^{3/2}} \times \\ \times \operatorname{Im} A\left(M_X^2, t\right), \tag{3}$$

where $\alpha_{fs}$ is the fine structure constant, $x = -t/2m\nu$ is the Bjorken variable, and $A\left(M_X^2, t\right)$ is the dual-Regge transition amplitude.

### 2.2. Step 2: Dual-Regge amplitude

The amplitude $A\left(M_X^2, t\right)$ in Eq. (3) is obtained from the unitarity and Veneziano duality [11]. According to the model of dual amplitude with Mandelstam analiticity (DAMA), the amplitude is expressed as the sum over Regge trajectories, ending up with the direct channel resonance decomposition

$$A\left(M_X^2, t\right) = a \sum_{n \geqslant 0} \frac{[f(t)]^{2(n+1)}}{2n + 0.5 - \alpha\left(M_X^2\right)}, \tag{4}$$

where $a$ is the normalization factor, $f(t) = (1 - t/t_0)^{-2}$ is the form factor of $\mathbb{P}p \to \mathbb{P}p$ system, $t_0$ is the model parameter. Finally, $\alpha\left(M_X^2\right)$ is the (nonlinear complex) baryonic resonance trajectory in $M_X^2$ channel, which allows one to account for a set of various resonances.

The imaginary part of the amplitude (4) needed for the structure function (3) is given by

$$\operatorname{Im} A\left(M_X^2, t\right) = a \sum_{n \geq 0} \left[f\left(t\right)\right]^{2(n+1)} \times \\ \times \frac{\operatorname{Im} \alpha\left(M_X^2\right)}{\left[2n + 0{,}5 - \operatorname{Re} \alpha\left(M_X^2\right)\right]^2 + \left[\operatorname{Im} \alpha\left(M_X^2\right)\right]^2}. \tag{5}$$

### Step 3: Proton trajectory

The last step in this journey is the nonlinear complex proton Regge trajectory $\alpha(M_X^2)$. It helps us to classify and understand the spectrum of excited states of proton and their decays, providing insights into the internal structure and dynamics of particles. These resonances indicate specific energy and angular momentum states, where the proton can undergo transitions to excited states before returning to the ground state. The real part of the trajectory $\operatorname{Re} \alpha(M_X^2)$ provides the relation between the mass of a resonance and its angular momentum (quantum number $J$). At the same time, the imaginary part of the trajectory provides the Breit–Wigner widths of the resonances

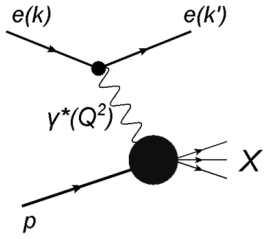


***Fig. 2.*** Deep inelastic scattering process $\gamma^* p \to X$ transition

$$\Gamma = \frac{\operatorname{Im} \alpha(M^2)}{M \operatorname{Re} \alpha'(M^2)}, \tag{6}$$

where $M$ is the resonance mass, $\operatorname{Re} \alpha'(M^2)$ denotes the first derivative (the slope) of the real part of the trajectory. The problem is to find a trajectory $\alpha(M^2)$ featuring both the almost linear real part (Fig. 3, *a*) and essentialy nonlinear imaginary part (Fig. 3, *b*), while holding the analiticity properties. Such trajectory has been extensively studied in [21] with the help of dispersion relations, which provides us with the expressions

$$\operatorname{Im} \alpha(s) = s^{\delta} \sum_n c_n \left(\frac{s - s_n}{s_n}\right)^{\operatorname{Re} a(s_n)} \theta(s - s_n), \tag{7}$$

$$\operatorname{Re} \alpha(s) = \alpha(0) + \frac{s}{\pi} \sum_n c_n \mathcal{A}_n(s), \tag{8}$$

where $c_n$ and $s_n$ are parameters to be fitted using the experimental data on resonances widths and masses, $\alpha(0)$ is the intercept of the real part of the trajectory. Note that the quantities $s$ and $s_n$ are nondimentionalized by $s_0 = 1$ GeV, so that resulting expressions are dimensionless, e.g., (7) and (8). The Heaviside step function $\theta(\cdot)$ is conventionally defined such that $\theta(0) = \frac{1}{2}$. The term $\mathcal{A}_n(s)$ in (8) emerges from a dispersion relation and is given by

$$\mathcal{A}_n(s) = \frac{\Gamma\left(1 - \delta\right)\Gamma\left(\lambda_n + 1\right)}{\Gamma\left(\lambda_n - \delta + 2\right)} s_n^{\delta - 1} \times$$

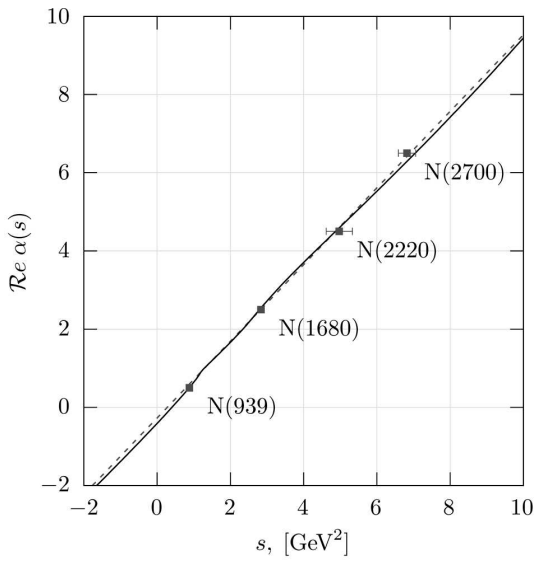


*a*

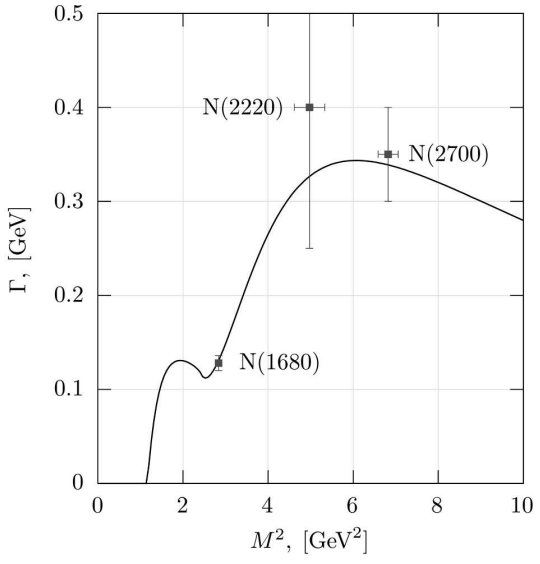


*b*

***Fig. 3.*** The real part of the fitted proton trajectory (8) (black solid line) and linear fit (red dashed line) (*a*). The fit of resonance widths (6) (solid line) and the experimental data from Tablle 1 (*b*). The fit [21] of the proton trajectory to N-resonances data

$$\times\, {}_2F_1\left(1, 1-\delta; \lambda_n - \delta + 2; \frac{s}{s_n}\right)\theta\left(s_n - s\right) +$$
$$+\left\{\pi s^{\delta-1}\left(\frac{s-s_n}{s}\right)^{\lambda_n}\cot\left[\pi\left(1-\delta\right)\right] -\right.$$
$$-\frac{\Gamma\left(-\delta\right)\Gamma\left(\lambda_n+1\right)}{\Gamma\left(\lambda_n-\delta+1\right)}\left(\frac{s_n^{\delta}}{s}\right)\times$$
$$\left.\times\, {}_2F_1\left(\delta-\lambda_n, 1; \delta+1; \frac{s}{s_n}\right)\right\}\theta\left(s_n - s\right), \qquad (9)$$

where $\delta$ is the dimensionless paramter to be fitted, $\Gamma(x)$ is the gamma function, ${}_2F_1(a,b;c,z)$ is the Gaussian hypergeometric function, $\cot(x)$ denotes cotangent function, and $\lambda_n = \mathrm{Re}\,\alpha(s_n)$.

Note that $\mathrm{Re}\,\alpha$ appears on the both sides of Eq. (8) through $\lambda_n$. Thus, (7), (8) and (9) are, in fact, functional equations, which significantly sophisticates the fitting procedure necessary to determine the values of the parameters $\alpha(0)$, $\delta$, $c_n$, and $s_n$, where $n = 1, 2, x$.

The baryons included in the trajectory are N(939), N(1680), N(2220), N(2700), and their properties depicted in Table 1. These resonances have been observed in the experiments studying of single diffraction dissociation processes, providing a framework for the study of SDD. The recursive fitting procedure of proton trajectory (7), (8) to the data for these resonances has been performed in [21].

*The fitting algorithm* can be summarized as follows. Due to the close-to-linear form of the real part of the trajectory, it is reasonable to start with the fit of the linear approximation of the real part $\alpha_{\mathrm{lin}}(s) = \alpha(0) + \alpha'(0)s$, which gives the initial values of $\lambda_n^{(0)} = \mathrm{Re}\,\alpha_{\mathrm{lin}}\left(s_n\right)$. Then the expression (6) for the widths of resonances is iteratively fitted to the experimental data Table 1. After each iteration, the values of $\lambda_n$ are updated $\lambda_n = \mathrm{Re}\,\alpha\left(s_n\right)$ using (8) with the updated values of parameters. The process is repeated until the sequence of trajectories converges. The resulting values of parameters are summarized in Table 2.

Using the values of parameters from Table 2, we plot the trajectory $\alpha(s)$ and ensure it match [21] (see Fig. 3). This completes the construction of the ex-

*Table 1.* **The baryons included in the fit [21] of trajectory $\alpha(s)$. The columns from left to right are: the baryon name, total angular momentum $J$, Breie–Wigner mass $M$, Breit–Wigner width $\Gamma$**

| Name | $J$ | $M$ (MeV) | $\Gamma$ (MeV) |
|---|---|---|---|
| N(939) | 1/2 | 939 | – |
| N(1680) | 5/2 | $1684 \pm 4$ | $128 \pm 8$ |
| N(2220) | 9/2 | $2230 \pm 80$ | $400 \pm 150$ |
| N(2700) | 13/2 | $2612 \pm 45$ | $350 \pm 50$ |

pression for differential cross-section for single diffraction dissociation (1).

Substituting $W_2$ from (3) into (1) we obtain

$$\frac{d^2\sigma}{dtdM_x^2}(M_x^2,t) = A_0\left(\frac{s}{M_x^2}\right)^{2\alpha_p(t)-2} \times$$
$$\times \frac{x(1-x)^2[F^p(t)]^2}{(M_x^2-m^2)(1-4m^2x^2/t)^{3/2}} \sum_{n=1}^{3}[f(t)]^{2n+2} \times$$
$$\times \frac{\operatorname{Im}\alpha(M_x^2)}{[2n+0{,}5-\operatorname{Re}\alpha(M_x^2)]^2+[\operatorname{Im}\alpha(M_x^2)]^2}, \qquad (10)$$

where $A_0 = 9a\beta^4/\pi\alpha_{fs}$ is the normalization factor that combines the factors $a$ and $\beta$ from (1) and (5). Other free parameter is $t_0$ of the form factor $f(t)$ appearing in the expression for the transition amplitude (4). The rest of parameters $\alpha(0), \delta, c_n, s_n$ $(n = 1, 2, x)$ are fixed from the trajectory fit Table 2. The values of $A_0$ and $t_0$ can be determined from the fit of the differential cross-section $d\sigma_{\mathrm{SDD}}/dt$ and total cross-section $\sigma_{\mathrm{SDD}}$. In the next section, we will analyze the behavior of the double differential cross-section (10) andwill discuss the applicability range of the model.

## 3. Model Behavior in the Resonance Region

In the study of the single diffraction dissociation processes, the regions of small and large missing masses $M_X$ offer distinct mechanisms of particle interactions. Here, we will focus on the small missing masses $M_X$, where the behavior of the cross-section is notably influenced by resonances within the structure functions. These resonances manifest themselves as peaks in the cross-section data, shaping the scattering processes observed at lower energies. In the present model, the resonances are accounted via the proton trajectory described in the previous section. This trajectory defines the behavior of the differential cross-section (10) in the $M_X$ region, where resonances appear (see Fig. 4).

As $M_X \to m$, the scattering process exhibits the elastic-like nature ($m$ is the proton mass), which significantly differs from the resonance production processes. The proper account for the contributions from the elastic and close-to-elastic processes requires a distinct model. Thus, we focus on the contributions from the resonance region only and *consider elastic processes as background contributions*. In the present

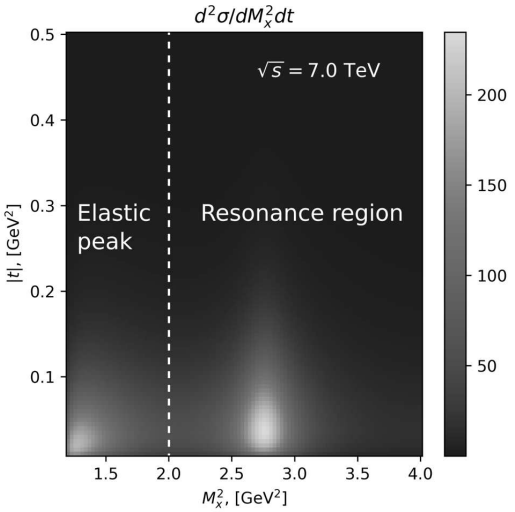


***Fig. 4.*** The differential cross-section $d^2\sigma/dtdM_X^2$ (10) in $t$, $M_X^2$ plane. There are two missing mass $M_X$ regions: elastic peak region ($M_X^2 < 2$ GeV$^2$) and the resonance region ($2\ \mathrm{GeV}^2 \leqslant M_X^2 \leqslant 8\ \mathrm{GeV}^2$)

model, the elastic contributions appear as the elastic peak in the differential cross-section as low $M_X$, as can be seen in Fig. 4. To avoid double counting in the elastic region, we follow [11] and consider $M_X^2 \geqslant 2$ GeV$^2$, which cuts elastic peak off. At the same time, at large missing masses $M_X$, the contributions of resonance productions expectedly reduce, making cross-section (10) neglectedly small for $M_X^2 > 8$ GeV$^2$. In this region, other Regge mechanisms come into play, but they are outside of the scope of the present work. This justifies what we call the *resonance region* $2\ \mathrm{GeV}^2 \leqslant M_X^2 \leqslant 8\ \mathrm{GeV}^2$.

It is important to mention that not only elastic processes can contribute to background. All other resonances which are not taken into account directly in this model are considered as a background as well. They can be added in a form of the contribution $B(M_X^2, t)$ to the differential cross-section. This function should decay quickly enough and does not diverge at infinity. For example, a common depen-

*Table 2.* **Parameters of proton trajectory $\alpha(s)$ obtained in [21] by fitting (6) to resonances data Table 1**

| | | |
|---|---|---|
| $\alpha(0) = -0.41$<br>$\delta = -0.46$ | $c_1 = 0.51$<br>$c_2 = 4.0$<br>$c_x = 4.6 \times 10^3$ | $s_1 = 1.16\ \mathrm{GeV}^2$<br>$s_2 = 2.44\ \mathrm{GeV}^2$<br>$s_x = 11.7\ \mathrm{GeV}^2$ |

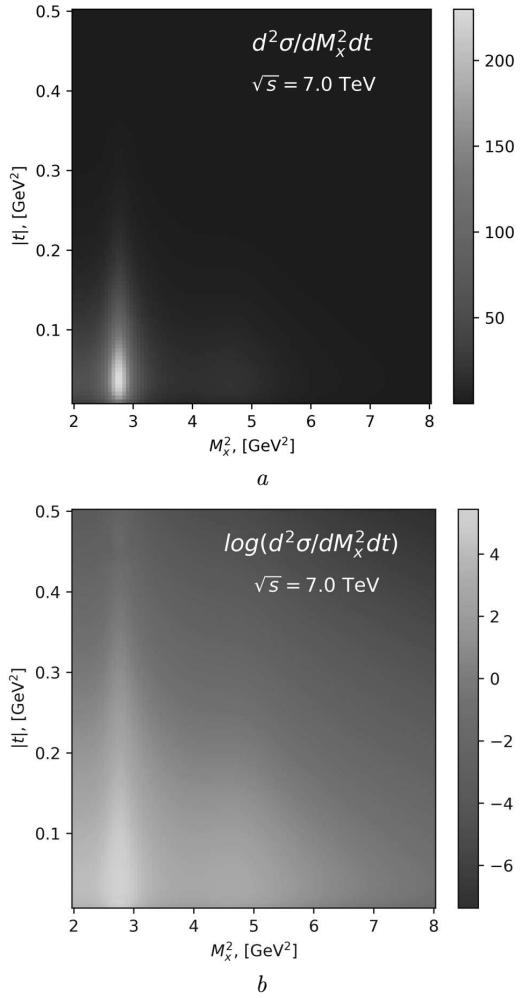


***Fig. 5.*** The differential cross-section $d^2\sigma/dtdM_X^2$ (10) in the $t$, $M_X^2$ plane ($a$), and its logarithm ($b$), plotted in the resonance region for $0 \leqslant -t \leqslant 0.5$ GeV$^2$

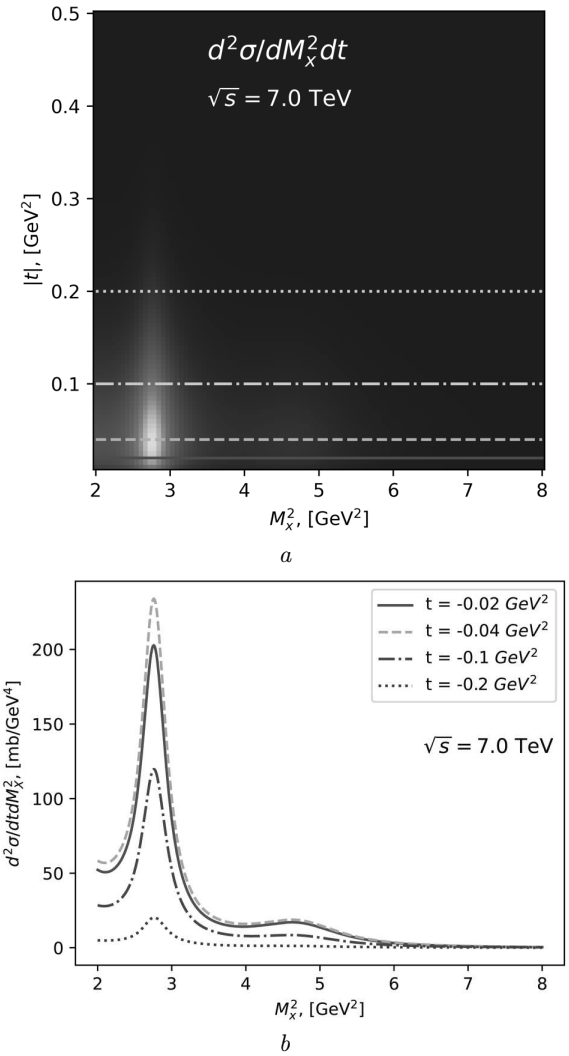


***Fig. 6.*** The differential cross-section $d^2\sigma/dtdM_X^2$ (10) in the $t$, $M_X^2$ plane in the resonance region for $0 \leqslant -t \leqslant 0.5$ GeV$^2$ (top), and multiple regular plots in $M_X^2$ at fixed values of $t$ (bottom)

dence on $M_X^2$ is usually chosen in a form $B(M_X^2) \sim 1/(M_X^2)^\eta$, where $\eta \geq 1$. Yet, we don't know the exact function $B(M_X^2, t)$, but we consider it to exist in a form which gives a constant value after the integration over $M_X^2$ and $t$.

So the final differential cross-section with additional background and resonances calculation from (10) reads as

$$\frac{d^2\widetilde{\sigma}}{dtdM_X^2}(M_X^2, t) = \frac{d^2\sigma}{dtdM_X^2}(M_X^2, t) + B(M_X^2, t). \quad (11)$$

The plots of resonance contribution to the double differential cross-section (10) in the resonance region are depicted on Figs. 5, 6, 7. The single peak in $M_X^2$ dimension is clearly visible in the resonance region. The unfitted values of the parameters used in this section are $A_0 = 10^3$ mb/GeV$^2$ and $t_0 = 0.71$ GeV$^2$.

## 4. Cross-Sections

In this section, we calculate differential and integrated cross-sections and fit them to the experimental data to find the values of parameters $A_0$ and $t_0$.

First, we integrate the double differential cross-section (11) over $M_X^2$ in resonance region to calculate

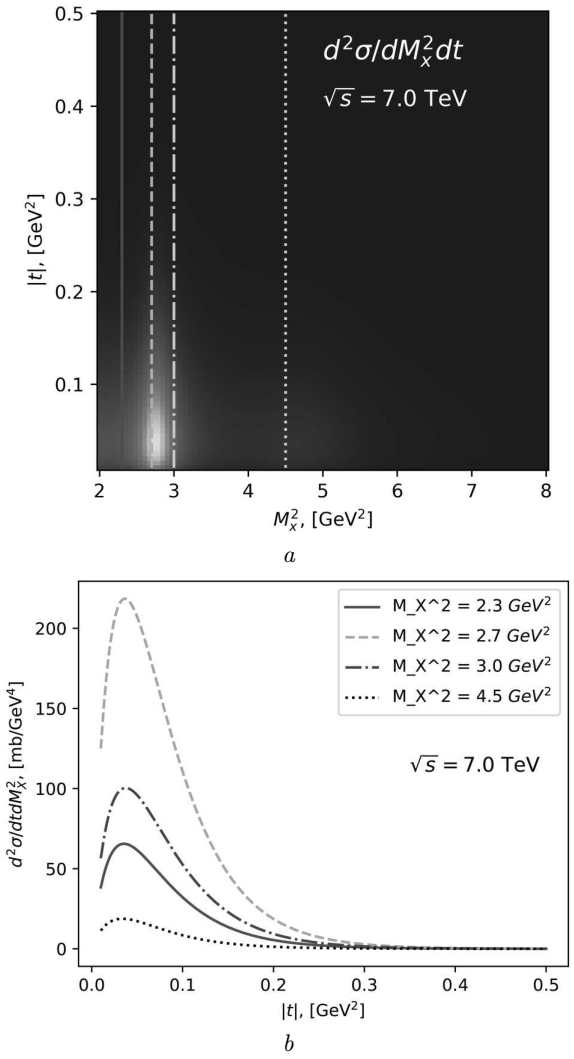


***Fig. 7.*** The differential cross-section $d^2\sigma/dtdM_X^2$ (10) in the $t$, $M_X^2$ plane in the resonance region for $0 \leqslant -t \leqslant 0.5$ GeV$^2$ (top), and multiple regular plots in $t$ at fixed values of $M_X^2$ (bottom)

the differential cross-section

$$\frac{d\sigma}{dt}(t) = \int_2^8 \frac{d^2\tilde{\sigma}}{dtdM_x^2}\left(t, M_x^2\right) dM_x^2 =$$

$$= \int_2^8 \frac{d^2\sigma}{dtdM_x^2}\left(t, M_x^2\right) dM_x^2 + b_0, \qquad (12)$$

where $b_0$ is the simple model of background contribution discussed in the previous section. Then we fit (12) to the experimental data [10] using the `ROOT` implementation of `Minuit` framework. The fitting procedure converges with $\chi^2/\text{d.o.f.} \approx 1.07$, providing the following values of the parameters: $A_0 = 35.58$ mb/GeV$^2$, $t_0 = 1.486$ GeV$^2$, and $b_0 = 8.2$ mb/GeV$^2$. The result of the fitting procedure is shown in Fig. 8.

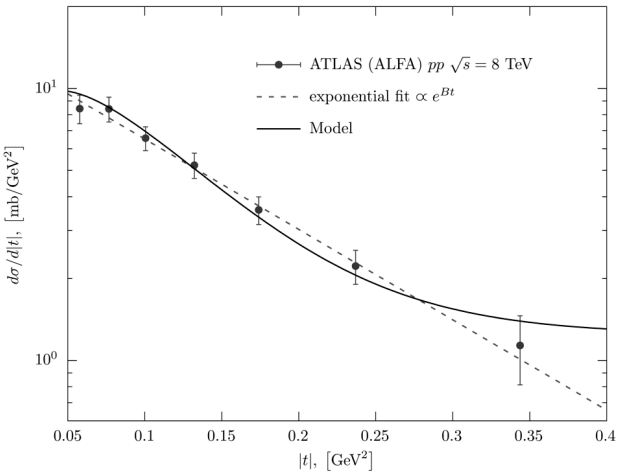


***Fig. 8.*** The differential cross-section $d\sigma/dt$ of single diffraction dissociation as a function of $|t|$. The dashed line is the exponential fit to the experimental data [10]. The solid line is the model fit with the constant background contribution $b_0$

The next step, is to integrate (12) over $t \in [0, 0.5]$ to calculate the cross-section

$$\sigma_{\text{SDD}} = \int_{-s}^{0}\int_2^8 \frac{d^2\sigma}{dtdM_X^2}\left(t, M_X^2\right) dM_X^2 dt + b, \qquad (13)$$

where $b$ is the background contribution. Note that we do not have any reliable model for the background; so, we relax the connection between $b_0$ and $b$ and fit them separately. The fit of differential cross-section $d\sigma/dt$ gives us the reasonable estimate for $t_0 = 1.486$ GeV$^2$, that we can use in the cross-section fit. The fitting procedure converges giving $\chi^2/\text{d.o.f.} = 14.03$ without background contribution, and providing the value of $A_0 = 565 \pm 3.11$ mb/GeV$^2$. Accounting for the constant background contribution $b$, gives us the better fit result $\chi^2/\text{d.o.f.} = 10.72$. The values of the parameters in this case are $A_0 = 378.43 \pm 16.68$ mb/GeV$^2$ and $b = 1.85 \pm 0.16$ mb/GeV$^2$.

## 5. Low Missing Mass Event Generation

The differential cross-sections fitted in the previous section provide facilities to generate events for low-missing-mass single diffractive processes.

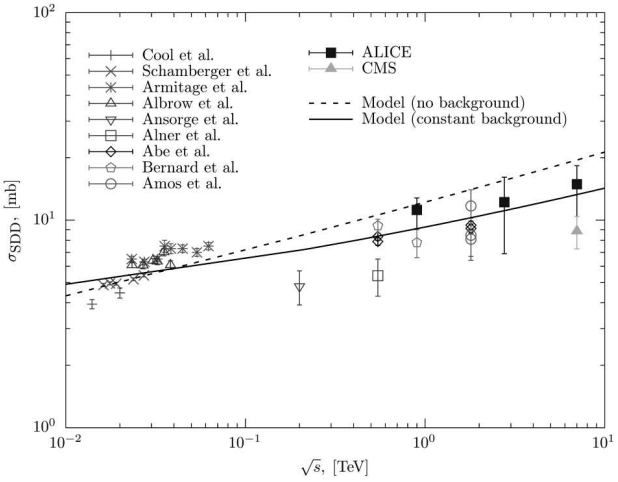


***Fig. 9.*** The single diffraction dissociation cross-section as a function of $\sqrt{s}$. The dashed line is the model fit to the experimental data [5–9, 22–28] without any background contribution. The solid line is the fit with the constant background contribution $b$

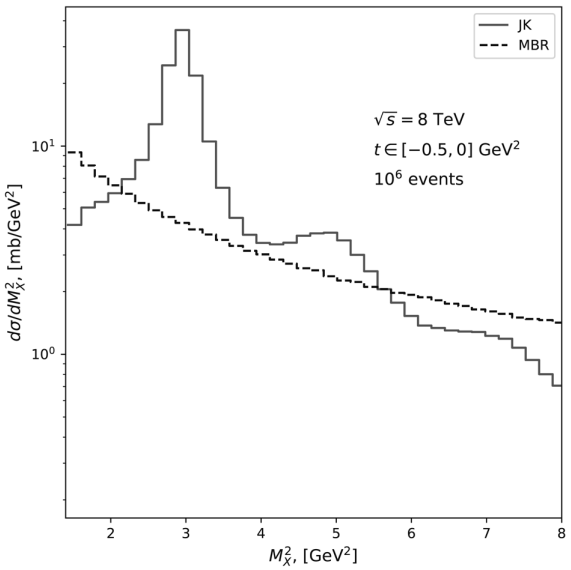


***Fig. 10.*** The comparison of the considered model against the MBR simulation in Pythia 8 at $\sqrt{s} = 7$ TeV

In this context, the four-momentum transfer squared $t$ and the squared mass $M_X^2$ of the dissociated system become random variables. The joint probability density of $t$ and $M_X^2$ is given by the double differential cross-section (10) at fixed $\sqrt{s}$

$$\rho\left(M_X^2, t\right) = \frac{1}{N}\frac{d^2\sigma}{dtdM_X^2}\left(M_X^2, t\right), \tag{14}$$

where $N = \sigma_{\mathrm{SDD}}\left(\sqrt{s}\right)$ is the normalizing factor ensuring unit total probability, and $\sigma_{\mathrm{SDD}}\left(\sqrt{s}\right)$ is the integrated single diffraction dissociation cross-section (13). As discussed in the previous section, we consider the domain of $M_X^2 \in [2, 8]$ GeV$^2$.

To generate an event, we sample a pair $(t, M_X^2)$ from the probability density (14). While this can be done in multiple ways (e.g., the acceptance-rejection method [29]), we follow the algorithm used in the Minimum Bias Rockefeller (MBR) simulation [30] implemented in Pythia 8 event generator. The idea is to begin by sampling a value of $M_X^2$ from the marginal probability density function

$$\rho_{M_X}(M_X^2) = \int\limits_{t_{\min}}^{0} \rho(M_X^2, t)\, dt = \\ = \frac{1}{N}\int\limits_{t_{\min}}^{0} \frac{d^2\sigma}{dtdM_X^2}(M_X^2, t)\, dt, \tag{15}$$

where $t_{\min} = -1$ GeV$^2$ defines the integration lower bound, cutting off the region of the small values of cross-section. The integral in (15) is calculated numerically.

Next, the value of $t$ is sampled from the conditional probability density function

$$\rho_t(t\,|M_X^2) = \frac{\rho(M_X^2, t)}{\rho_{M_X}(M_X^2)}. \tag{16}$$

Finally, the generated pair $(t, M_X^2)$ together with the Mandelstam variable $s$ gives us the four-momenta of the proton and dissociated system in the final state, which can be calculated from the relativistic kinematics of two-body scattering.

In the resonance region at low missing masses a significant difference between two approaches can be seen. The MBR simulation demonstrates the monotonically decreasing behavior of the cross-section in the region of low missing masses. Whereas considered model predicts highly non-monotonic dependency with multiple peaks corresponding to the resonances.

## 6. Summary

The in-depth examination of the differential cross-sections behavior within the resonance region with a constant background contribution is performed, particularly at low missing masses $M_X$. The refinement

of model parameters through the incorporation of new experimental data is discussed, improving the accuracy and predictive capabilities. The fits of differential and total cross-sections were performed using C++ programs within the ROOT framework, specifically employing Minuit for parameter optimization. Results are presented as numerical values of parameters, goodness-of-fit metrics, and graphical representations. The most recent data from ATLAS, ALICE, CMS were used for calculations.

It was shown that a better fit of the new data for the total cross-section can be obtained by considering the constant background contribution $b$. On the other hand, such model struggles to describe the data for the differential cross-section out of the resonance region. This is due to the fact that a constant contribution to the differential cross-section doesn't give an accurate description at higher values of momentum transfer $t$. In this region, the cross-section should go to 0, instead of the constant background $b_0$ gives nonphysical behavior of the system. Simple exponential model shows better results in this case. The proper modeling of the background contributions could potentially yield significant improvements in the accuracy of the results and should be a focus of a future research. For example, the more sophisticated background model from [31] can be used for this purpose.

A constant-background model was used for the event generation simulations in Pythia 8. The model was compared to the MBR methods in the resonance region at low missing masses. It was shown that, unlike the MBR method, our method exhibits nonmonotonic behavior, characterized by peaks that describe resonances.

*We are grateful to L.L. Jenkovszky for a valuable discussion. This project has received the funding through the EURIZON project, which is funded by the European Union under grant agreement No. 871072.*

1. K.A. Goulianos. Diffractive Interactions of Hadrons at High-Energies. *Phys. Rept.* **101**, 169 (1983).
2. E. Feinberg, I. Pomeranchuk. High Energy Inelastic Diffraction. Phenomena. *Nuovo Cimento Suppl.* **3**, 652 (1956).
3. M.L. Good, W.D. Walker. Diffraction disssociation of beam particles. *Phys. Rev.* **120**, 1857 (1960).
4. G. Antchev *et al.* (TOTEM Collaboration). Double diffractive cross-section measurement in the forward region at the LHC. *Phys. Rev. Lett.* **111**, 262001 (2013).
5. V. Khachatryan *et al.* Measurement of diffractive dissociation cross sections in $pp$ collisions at $\sqrt{s} = 7$ TeV. *Phys. Rev. D* **92**, 012003 (2015).
6. M.G. Albrow *et al.* Inelastic diffractive scattering at the CERN ISR. *Nuclear Physics B* **108**, 1 (1976).
7. R.E. Ansorge *et al.* Diffraction Dissociation at the CERN Pulsed Collider at CM Energies of 900-GeV and 200-GeV. *Z. Phys. C* **33**, 175 (1986).
8. D. Bernard *et al.* The cross section of diffraction dissociation at the cern SPS collider. *Phys. Lett. B* **186**, 227 (1987).
9. B. Abelev *et al.* Measurement of inelastic, single- and double-diffraction cross sections in protonпїSproton collisions at the LHC with ALICE. *Europ. Phys. J. C* **73**, 2456 (2013).
10. The ATLAS collaboration, G. Aad *et al.* Measurement of differential cross sections for single diffractive dissociation in $\sqrt{s} = 8$ TeV pp collisions using the ATLAS ALFA spectrometer. *J. High Energy Phys.* **2020**, 42 (2020).
11. L.L. Jenkovszky, O.E. Kuprash, J.W. Lämsä, V.K. Magas, R. Orava. Dual-Regge approach to high-energy, low-mass diffraction dissociation. *Phys. Rev. D* **83**, 056014 (2011).
12. M. Baker, K.A. Ter-Martirosyan. Gribov's Reggeon calculus: Its physical basis and implications. *Phys. Repo.* **28**, 1 (1976).
13. P.D.B. Collins. *An Introduction to Regge Theory and High Energy Physics* (Cambridge University Press, 2023) [ISBN: 978-1-00-940326-9].
14. K. Hagiwara *et al.* (Particle Data Group). Review of particle properties. *Phys. Rev. D* **66**, 010001 (2002).
15. L. Jenkovszky, R. Schicker, I. Szanyi. Elastic and diffractive scatterings in the LHC era. *Int. J. Mod. Phys. E* **27**, 1830005 (2018).
16. I. Szanyi, L. Jenkovszky, R. Schicker, V. Svintozelskyi. Pomeron/glueball and odderon/oddball trajectories. *Nucl. Phys. A* **998**, 121728 (2020).
17. L. Jenkovszky, R. Schicker, I. Szanyi. Dip-bump structure in proton's single diffractive dissociation at the large hadron collider. *Universe* **10**, 208 (2024).
18. S. Donnachie, G. Dosch, P. Landshoff, O. Nachtmann. *Pomeron Physics and QCD* (Cambridge University Press, 2002) [ISBN: 9780511534935].
19. R. Fiore, A. Flachi, L.L. Jenkovszky, A.I. Lengyel, V.K. Magas. Kinematically complete analysis of the CLAS data on the proton structure function $F_2$ in a Regge-dual model. *Phys. Rev. D* **69**, 014004 (2004).
20. F. Halzen, Alan D. Martin. *Quarks and leptons* (John Wiley & Sons, 1984) [ISBN: 0-471-88741-2].
21. R. Fiore, L.L. Jenkovszky, F. Paccanoni, A. Prokudin. Baryonic Regge trajectories with analyticity constraints. *Phys. Rev. D* **70**, 054003 (2004).
22. R.L. Cool, K. Goulianos, S. L. Segler, H. Sticker, S.N. White. Diffraction Dissociation of $\pi^{\pm}$, $K^{\pm}$,and $p^{\pm}$ at 100 and 200 GeV/c. *Phys. Rev. Lett.* **47**, 701 (1981).
23. R.D. Schamberger, J. Lee-Franzini, R. McCarthy, S. Childress, P. Franzini. Mass spectrum of proton-proton inelas-

tic interactions from 55 to 400 GeV/c at small momentum transfer. *Phys. Rev. D* **17**, 1268 (1978).
24. J.C.M. Armitage *et al.* Diffraction dissociation in proton-proton collisions at ISR energies. *Nucl. Phys. B* **194**, 365 (1982).
25. G.J. Alner *et al.* UA5: A general study of proton-antiproton physics at $\sqrt{s} = 546$ GeV. *Phys. Rep.* **154**, 247 (1987).
26. F. Abe *et al.* Measurement of $p\bar{p}$ single diffraction dissociation at $\sqrt{s} = 546$ and 1800 GeV. *Phys. Rev. D* **50**, 5535 (1994).
27. N.A. Amos *et al.* A luminosity-independent measurement of the pp total cross section at $\sqrt{s} = 1.8$ TeV. *Phys. Lett. B* **243**, 158 (1990).
28. N.A. Amos *et al.* Diffraction dissociation in pp collisions at $\sqrt{s} = 1.8$ TeV. *Phys. Lett. B* **301**, 313 (1993).
29. L. Devroye. *Non-Uniform Random Variate Generation* (Springer, 1986) [ISBN: 0-387-96305-7].
30. R. Ciesielski, K. Goulianos. MBR Monte Carlo Simulation in PYTHIA8. *PoS* **ICHEP2012**, 301 (2013).
31. L.L. Jenkovszky, O.E. Kuprash, R. Orava, A. Salii. Low missing mass, single and double diffraction dissociation at the LHC. *Physics of Atomic Nuclei* **77**, 1463 (2014).

Received 06.04.25

*О.С. Потієнко, Д.В. Журавель,*
*Н.О. Чудак, Д.М. Рябов*

МОДЕЛЮВАННЯ ОДИНАРНОЇ ДИФРАКЦІЙНОЇ ДИСОЦІАЦІЇ В РЕЗОНАНСНІЙ ОБЛАСТІ ПРИ ВИСОКИХ ЕНЕРГІЯХ

Представлено модель одинарної дифракційної дисоціації, яка заснована на принципі дуальності, в області низьких значень маси з урахуванням нових експериментальних даних. Ключовою особливістю моделі є використання нелінійної траєкторії протона у формалізмі Редже, що дозволяє врахувати внесок резонансних станів у повні та диференціальні перерізи. Такий підхід сприяє класифікації та глибшому розумінню спектра збуджених станів протона й особливостей їх розпадів, що, своєю чергою, дає змогу дослідити внутрішню структуру та динаміку частинок. Аналізується поведінка диференціального перерізу в резонансній області при малих значеннях маси $M_x$. Всі інші резонанси, які явно не враховуються, описуються шляхом введення сталого внеску від фону. Обговорюється обґрунтованість та допустимість такого припущення. Параметри моделі уточнюються з урахуванням нових експериментальних даних.

*Ключові слова*: одинарна дифракційна дисоціація, структурна функція протона, область резонансів, малі маси, переріз, генерація подій.